THE EFFECTS OF COMPRESSION ON ULTRA WIDE-BAND RADAR SIGNALS

B. McGinley[1, 2, *], M. O'Halloran[1, 2], R. Conceicao[1, 2], G. Higgins[1, 2], E. Jones[1, 2], and M. Glavin[1, 2]

[1]College of Engineering and Informatics, National University of Ireland Galway, University Road, Galway, Ireland

[2]Bioelectronics Research Cluster, National Centre for Biomedical Engineering Science (NCBES), National University of Ireland Galway, University Road, Galway, Ireland

Abstract—Over the past ten years, Ultra Wideband (UWB) Radar has been widely investigated as a biomedical imaging modality, used to detect early-stage breast cancer and to continuously monitor vital signs using both wearable and contactless devices. The advantages of the technology in terms of low-power requirements and non-ionising radiation are well recognised, with the technology being applied to a range of non-invasive medical applications, from respiration to heart monitoring. Across all these applications, there is a strong necessity to efficiently manage the large quantities of UWB data which will be captured. For wearable devices in particular, the efficient compression of UWB data allows the monitoring system to conserve limited resources such as memory and battery capacity, by reducing data storage and in some cases transmission requirements. In contrast to lossless compression techniques, lossy compression algorithms can achieve higher compression ratios and consequently greater power savings, at the expense of a marginal degradation of the reconstructed signal. This paper compares the lossy JPEG2000 and Set Partitioning In Hierarchical Trees (SPIHT) algorithms for UWB signal compression. This study examines the effects of lossy signal compression on an UWB breast cancer classification algorithm. This particular application was chosen because the classification algorithm relies heavily on shape and surface texture detail embedded in the Radar Target Signature (RTS) of the tumour, and therefore will provide both a robust and easily quantifiable test platform for the compression algorithms. The

* Corresponding author: Brian McGinley (brianmcginley@gmail.com).

study will evaluate the performance of the classification algorithm as a function of Compression Ratio (CR) and Percentage Root-mean-square Difference (PRD) between the original and reconstructed UWB signals.

1. INTRODUCTION

Ultra Wideband (UWB) Radar is one of the most promising emerging imaging modalities. UWB imaging and monitoring is based on the detection of reflected UWB signals from tissue-boundaries within the human body. These boundaries reflect UWB signals due to difference in dielectric properties between these various constituent tissues at microwave frequencies. The wide frequency-spectrum of the UWB signal means they are relatively robust to interference, while also allowing for very fine spatial resolution, making the technology ideal breast cancer detection and classification [1–17], heart and respiration monitoring [18–21]. Furthermore, UWB Radar uses low-power non-ionising radiation and is therefore a safe method for imaging and continuous monitoring. However, many UWB monitoring devices generate large quantities of data and therefore bio-signal data compression will be an important means of power conservation in wearable UWB monitoring systems. Approaches to dealing with this data generally fall into two broad categories: Storage or transmission. Storage implies saving the information locally on the device, while transmission removes the need for large amounts of local storage, but requires an integrated wireless transmitter to facilitate data communication to a central location. An essential advantage of transmission is that an immediate clinical response can be initiated. Transmission, however, is expensive from a power-perspective and battery-life consequently suffers. A wireless sensor network for ambulatory health monitoring is described in [22], where the authors state that "95% of the sensor's power consumption can be attributed to wireless communications". With this in mind, data compression algorithms should be examined to reduce the amount of UWB information to be transmitted/stored, considerably reducing the power and memory requirements of ambulatory UWB devices in particular.

There are two main types of compression algorithm: lossless and lossy. Lossless compression can achieve perfect reconstruction of the compressed data. While this is a desirable objective, it limits the Compression Ratio (CR), and hence the power/memory savings that can be attained. Conversely, lossy compression does not allow for perfect reconstruction of the data, but has the advantage that much higher CRs can be obtained. Therefore, it is desirable to use a

compression algorithm which maximises CR, while also maximising signal fidelity. JPEG2000 [23] and Set Partitioning In Hierarchical Trees (SPIHT) [24] are state of the art compression algorithms, which encode Discrete Wavelet Transform (DWT) output coefficients into a binary stream. The DWT provides good localisation of the signal's energy components from both a time and frequency perspective. The DWT coefficients therefore represent the signal's energy more compactly than the original representation. JPEG2000 and SPIHT efficiently encode DWT coefficients into a binary stream suitable for transmission or storage. This paper compares the JPEG2000 and SPIHT algorithms for UWB signal compression.

In order to quantitatively examine the performance of these compression algorithms on UWB signals, the JPEG2000 and SPIHT algorithms are applied to UWB signals used for breast cancer classification. The reasons that these signals were chosen as a test platform for the compression algorithms are twofold: firstly, tumour classification algorithms rely on shape and surface-texture information embedded in the Radar Target Signature of the tumour, and therefore the classification algorithm is very sensitive to errors in the signal reconstruction process; secondly, the classification accuracy provides a easily quantifiable measure to evaluate the performance of the compression algorithms. This study looks at the compression performance of each algorithm, both in terms of reconstructed signal fidelity at a particular CR and the percentage accuracy of the tumour identification classifier with varying degrees of compression. Signal fidelity is quantified by the Percentage Root-mean squared Difference (PRD) between original and reconstructed signals. The remainder of the paper is organised as follows: Section 2 describes both the JPEG2000 and SPIHT compression algorithms; Section 3 describes the simulation setup, while Section 4 presents the results and corresponding conclusions.

2. COMPRESSION ALGORITHMS

Transform-based compression involves projecting a signal onto a suitable basis, before the projected coefficients are compressed and encoded. This projection allows the data to be expressed much more concisely than in its original form. The Fourier and Discrete Cosine transforms employ stationary waveforms as basis functions. Alternatively, the DWT employs non-stationary waveforms as basis function to extract both time and frequency information from a signal [25]. JPEG2000 and SPIHT are state of the art compression algorithms, which encode DWT output coefficients into a binary

stream, for transmission or storage.

2.1. Discrete Wavelet Transform (DWT)

The DWT [26, 27] expresses a signal as a weighted sum of basis functions. These bases are composed of dilated and translated versions of a function, known as the mother wavelet. This transformation (projection of the original signal onto the basis functions) produces an alternative representation of the original signal, expressed as coefficients of the set of basis functions. The mother wavelet is translated and varied in scale to extract both time and frequency information from the signal. Basis functions associated with large scales extract low-frequency information from the signal, while small scales extract high-frequency or fine-detail components. The DWT coefficients $c_{m,k}$ are defined as the inner product of the original signal $x(n)$ and the selected basis functions $\psi_{m,k}$, where m controls the wavelet's scale and k controls the wavelet's translation (1).

$$c_{m,k} = \langle x(n), \psi_{m,k} \rangle \tag{1}$$

These wavelet coefficients provide an alternative representation of the original signal, giving good localisation of the signal's energy components from both a time and frequency perspective. An efficient implementation of the DWT for discrete-time signals consists of recursive decomposition of the original signal using quadrature mirror low-pass and high-pass filters [28]. Following filtering and decimation of the filters' outputs by a factor of two, the process of low and high-pass filtering is reapplied in a cascaded fashion to the decimated output of the low-pass filter. An interesting by-product of recursive wavelet decomposition is the temporally oriented tree structure produced, when each of the levels of the detail coefficients are arranged in order of frequency. A single coefficient in one layer corresponds temporally to two coefficients in the next layer, as a result of the downsampling employed. These temporal relationships are illustrated by arrows in Figure 1. The higher layers in this temporal tree contain more low-frequency information. Since most of a signal's energy is usually focused in the low-frequency end of the spectrum, coefficients generally decrease in magnitude from top to bottom within the tree. It is these temporal and magnitude relationships between coefficients that are exploited by wavelet compression algorithms, such as SPIHT.

2.2. Set Partitioning in Hierarchical Trees (SPIHT)

SPIHT is a state-of-the-art wavelet-based compression algorithm, originally proposed by Said and Pearlman [24]. The SPIHT algorithm
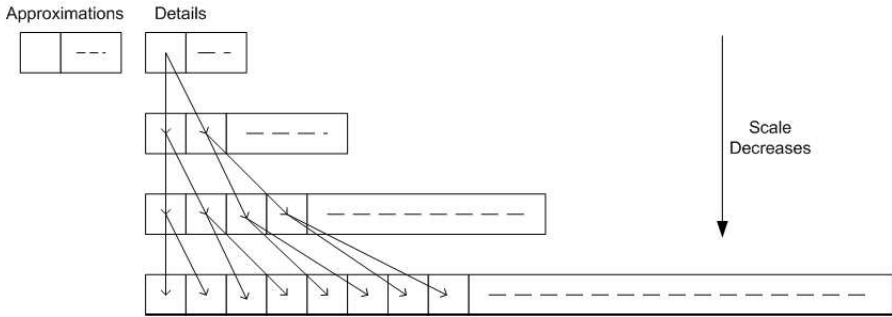
Figure 1. The DWT output arranged in a temporally oriented binary tree structure.

operates on the temporally oriented binary hierarchical wavelet tree (Figure 1), and benefits from the fact that coefficients generally decrease in magnitude from top to bottom. SPIHT scans the wavelet tree progressively according to a threshold t, which is initially selected according to (2). This threshold is reduced by a factor of 2 at each iteration of the algorithm.

$$t_0 = 2^{\lfloor \log_2(\max_{(i)} |C_i|) \rfloor} \tag{2}$$

SPIHT maintains wavelet coefficients in three lists, known as the List of Insignificant Points (LIP), the List of Insignificant Sets (LIS) and the List of Significant Points (LSP). The SPIHT algorithm recursively performs two passes of these coefficients at each threshold in order to encode the wavelet information. The first pass, known as the sorting pass, assigns each coefficient to a list depending on the coefficient's significance. A coefficient can either be significant, insignificant or part of an insignificant set.

Following the step of sorting the coefficients into their respective lists, the second pass, known as the refinement pass compares coefficients on the LSP to the threshold, and outputs a single bit depending on their significance. As the bits are ordered by importance (with the most significant bits encoded first), the encoder can terminate encoding at any point. This ability to gradually reconstruct an encoded signal using a partial bit-stream is known as embedded encoding. This approach allows for exact bit-rate control and means that the signal can be reconstructed to a deterministic fidelity at the decoder, using the transmitted bit-stream.

2.3. JPEG2000

JPEG2000 is a transform-based compression algorithm, intended for both lossless and lossy compression of images. JPEG2000 Part 1 was ratified by the Joint Photographic Experts' Group in 2000 [29] and was designed to replace the older JPEG file format with more advanced features, including: superior low bit-rate performance, lossless and lossy compression and good error-resilience [23]. Part 1 of the JPEG2000 standard includes the specifications for the core coding system. These core components include: Discrete Wavelet Transform (DWT), Quantisation and an Arithmetic Coder.

In addition to the core elements of the JPEG2000 Part 1 Standard, a thresholding step similar to that used in [30], is incorporated in this research to increase compression gains. This thresholding step is performed following quantisation. Coefficient values below the pre-selected threshold are deemed "insignificant" and are set to zero. The greater the number of coefficients with the same value, the more efficiently the AC can encode them and thus; the CR and accuracy of the reconstructed signal may be controlled.

A static Probability Density Function (PDF), constructed at different thresholds over the entire UWB database, is employed to encode each frame. The PDF is centred about zero, with the number of zero coefficients rising as the threshold increases.

3. SIMULATION SETUP

In this section, the Gaussian Random Spheres method, used to model the shape and surface texture of tumours is described, before the Finite-Difference Time-Domain (FDTD) method used to simulate the propagation and reflection of UWB signals in the breast is presented. Finally, the compression preprocessing and performance metrics are also described.

3.1. Gaussian Random Spheres & FDTD model

Tumours present different physical characteristics based on their nature, i.e., whether they are benign or malignant. The most relevant features from the perspective of UWB imaging are size, shape and texture of surface, as these are characteristics that most significantly influence the RTS of tumours. Benign tumours typically have smooth surfaces and have spherical, oval or at least well-circumscribed contours. Conversely, malignant tumours usually present rough and complex surfaces with spicules or microlobules, and their shapes are typically irregular, ill-defined and asymmetric [31]. Shape and texture

of the surface of a tumour are the two most important characteristics that will help differentiate between a benign and a malignant tumour. The tumour models are based on the Gaussian Random Spheres (GRS) method [32, 33]. GRS can be modified mathematically to model both malignant and benign tumours by varying the mean radius α and the covariance function of the logarithmic radius. The shape is determined by the radius vector, $\mathbf{r} = r(\theta, \psi)$, which is described in spherical coordinates (r, θ, ψ) by the spherical harmonics series for the logradius $s = s(\theta, \psi)$:

$$r(\theta, \psi) = \alpha \exp \left[s(\theta, \psi) - \frac{1}{2}\beta^2 \right] \tag{3}$$

$$s(\theta, \psi) = \sum_{l=0}^{\infty} \sum_{m=-l}^{l} s_{lm} Y_{lm}(\theta, \psi) \tag{4}$$

In the equations above, β is the standard deviation of the logradius, s_{lm} are the spherical harmonics coefficients and Y_{lm} are the orthonormal spherical harmonics. Three different tumour models at two different sizes are considered in this paper. Malignant tumours are represented
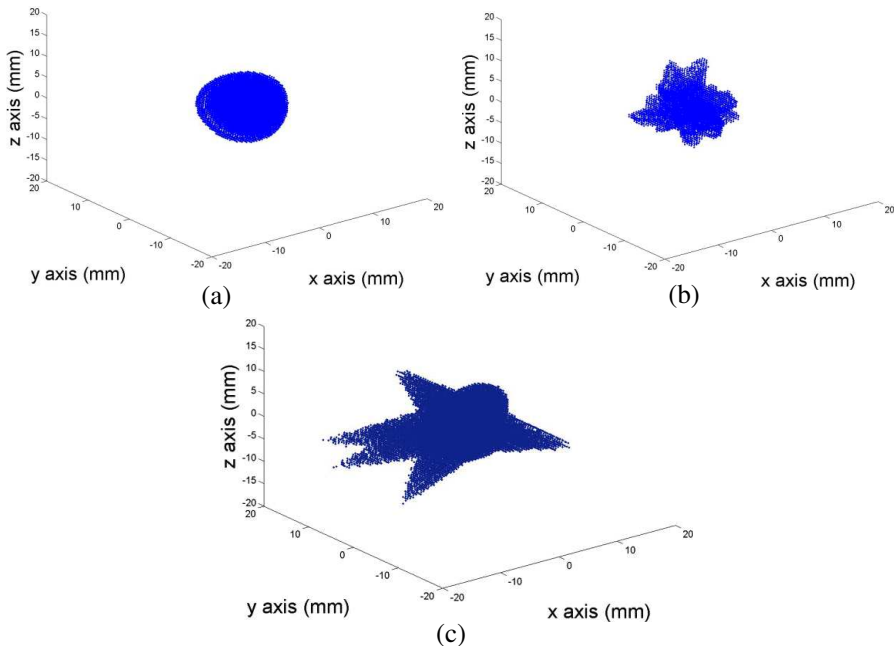

Figure 2. (a) Benign, (b) macrolobulated, and (c) malignant tumour model.

by spiculated and microlobulated GRS, whereas benign tumours are modelled by smooth GRS. Microlobulated and smooth GRS are obtained by varying the correlation angle from low to high. Spiculated GRS are obtained by adding 3, 5 or 10 spicules to smooth GRS. The average radius of all types of spheres are 2.5 and 7.5 mm. Between all sizes and shapes, the number of tumour models developed was 190. A sample of each of the types tumour models is shown in Figure 2.

The tumours are placed in a 3D Finite-Difference Time-Domain (FDTD) model. The FDTD model has a 0.5 mm cubic grid resolution and the backscattered signals were generated through a Total-Field/Scattered-Field (TF/SF) structure, in which the tumours are completely embedded in the Total Field (TF) [34]. The TF/SF region has the following dimensions: the Scattered Field (SF) is a square geometric prism with square bases measuring 153.5 mm on the side and the height measuring 137.5 mm. The TF is located at the centre of the SF and is represented by a 50 mm-sided cube (the origin of the SF and the TF are at the point $(0, 0, 0)$ mm). The dielectric properties of both adipose and cancerous breast tissue are incorporated
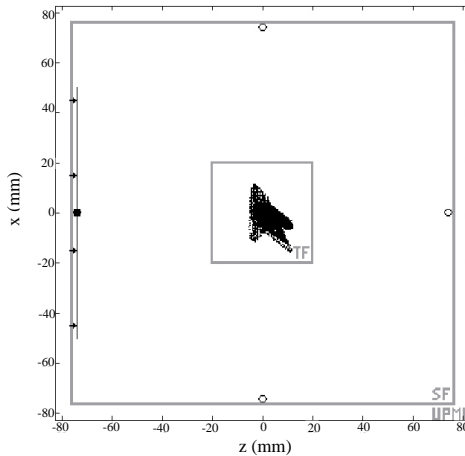

Figure 3. Cross-section of the 3D FDTD space lattice partitioned into Total Field (TF), Scattered Field (SF) and UPML regions, for a homogeneous breast model. The target, a spiculated tumour located at the centre of the TF in this example, is illuminated by a pulsed plane wave propagating in the $+z$ direction (represented by a dark line) and backscatter is recorded at the first observer location: $(0, 0, -74)$ mm (represented by a filled circle). All four observation points are represented by small circles in the image.

using a Debye model, based on the dielectric properties established by Lazebnik et al. The TF/SF region is terminated with a 6 mm-layer Uniaxial Perfectly Matched Layer (UPML) which suppresses any boundary reflections [35].

A pulsed plane wave is transmitted towards the target from four different equidistant angles (0, 90, 180 and 270°) and the resulting cross-polarised backscatter is recorded and analysed from four observation points located at: (0, 0, −74), (−74, 0, 0), (0, 0, 74) and (74, 0, 0) mm in (x, y, z) axes. The incident pulse is a modulated Gaussian pulse with center frequency at 6 GHz where the $1/e$ full temporal width of the Gaussian envelop was 160 ps. For two transmitters, the pulse is linearly polarised in the x-y plane and transmitted in the z direction, and for the remaining transmitters, the pulse is polarised in the y-z plane and transmitted in the z direction. Each observation point is located in the Scattered Field at a distance of 74 mm from the center of the tumour, which is located at the centre of the Total Field. The acquired backscattered recorded signals are then downsampled from 1200 GHz to 75 GHz. Figure 3 shows a representation of the TF/SF grid, with the location of the origin of the first incident plane wave and respective observer point as well as the position of the tumour.

3.2. Preprocessing

A total of 190 tumour models were considered (95 of size 2.5 mm and 95 of size 7.5 mm). Within that group, there were 95 type 1 tumours (malignant), 47 type 2 tumours (macrolobulated benign) and 48 type 3 tumours (smooth benign). In order to extract the most relevant features for classification, Principal Component Analysis (PCA) is applied to the backscattered signals.

As a first step in UWB signal compression, a 7-level DWT decomposition (using the CDF 9/7 biorthogonal wavelet [36]) was employed, since it was observed to concentrate the signal's energy in the fewest number of wavelet coefficients. Following transformation, wavelet coefficients are quantised to a signed 11-bit resolution, using a standard integer quantisation method and then passed to the two compression algorithms under investigation. SPIHT is implemented as described in [37]. The embedded SPIHT bit-stream is truncated to provide reconstructions at compression ratios ranging from 2 to 70. The JPEG2000 thresholding step, described above, is performed for threshold values ranging from zero to 360.

Next, a direct "tumour-type" classifier, based on Support Vector Machines (SVM), classifies each tumour as either benign or malignant. Similar tumour classifiers have been previously examined

by Conceicao et al. [15]. In order to evaluate the SVM classifier, the entire data-set is randomly shuffled and divided into 75%-25% training and test groups respectively. This classification process is repeated 10 times and the average performance of each classifier is calculated. The classification performance is then evaluated across a range of different CRs. The performance metrics are described in Section 3.3.

3.3. Metrics

Evaluation of the compression algorithms is based upon three metrics:

- Compression Ratio (CR)
- Percentage Root mean square Difference (PRD)
- Classifier Accuracy

The CR describes the compression algorithms' efficiency in representing the original data. The CR for each UWB frame is calculated as:

$$\text{CR} = \frac{Fr_s * Q_o}{b} \tag{5}$$

where Fr_s refers to the frame size used for performing compression (512 samples), Q_o refers to the quantisation applied to the original signal during sampling (16 bits) and b is the number of bits representing the compressed signal.

With regard to signal fidelity, the quality of compression is dictated by the reconstructed signal's similarity to the original. The measure of distortion is quantified by employing the PRD measure (6) [38]. PRD is calculated by expressing the difference between original and reconstructed signals, relative to the original signal's mean, as follows:

$$\text{PRD} = \frac{||\text{x}_\text{o} - \text{x}_\text{r}||}{||\text{x}_\text{o}||} \tag{6}$$

where x_o and x_r are the original and reconstructed signals, respectively, and $||x||$ represents the Euclidean or L_2 norm of x. Finally, the Classifier Accuracy is a measure (expressed as a percentage) of the total number of tumours correctly classified as either benign or malignant.

4. RESULTS & CONCLUSIONS

UWB signal compression algorithms could potentially be used in the development of a variety of UWB systems, ranging from breast cancer detection and classification, to vital sign monitoring, and early warning systems for Sudden Infant Death Syndrome. In order
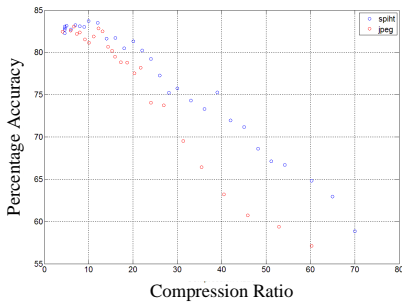
Figure 4. Plot of Classifier Accuracy versus Compression Ratio for JPEG2000 and SPIHT.
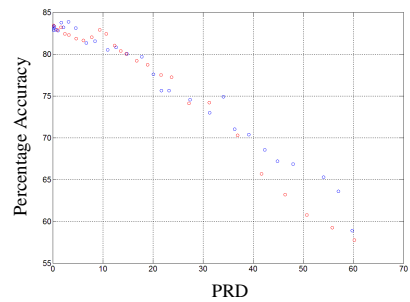
Figure 5. Plot of Classifier Accuracy versus PRD for JPEG2000 and SPIHT.

to investigate the effect of UWB signal compression, the SPIHT and JPEG2000 compression algorithms are applied to the UWB data at varying CRs before the reconstructed signals are classified. As a baseline, the Classification Accuracy before compression was established and found to be 89.16%. Classification Accuracy versus CR for both JPEG2000 and SPIHT is shown in Figure 4. Results indicate that CRs of up to 20 are achievable using SPIHT and up to 15 using JPEG2000 while still maintaining a classification accuracy of above 80%. Beyond these CRs, classifier performance degrades. This is an interesting result considering that tumour classification, which relies on fine shape detail, can be performed with $\frac{1}{20}$th of the original data. Although both algorithms are comparable in maintaining signal fidelity at low CRs, SPIHT outperforms JPEG2000 in achieving a lower PRD (reconstruction error) at higher CRs (above 20). SPIHT thereby retains more diagnostically relevant information than JPEG200 for a given CR. This is because SPIHT employs an embedded encoding scheme, whereby the most relevant information is contained at the beginning of the bitstream. This contrasts with JPEG2000 where no such prioritisation of information is employed. SPIHT's progressive ordering of information means that information is represented more concisely as CR increases. In addition, JPEG2000 has an added transmission overhead, associated with the PDF employed for encoding. With JPEG, the entire set of coefficients must be encoded in the message while SPIHT only encodes the most relevant information within the bits allocated.

While CR vs. Classification Accuracy allows a compression comparison of both algorithms, it does not inform on the PRD that can be tolerated by the classification algorithm. Figure 5 illustrates Classifier Accuracy versus PRD for both JPEG2000 and

SPIHT. Both algorithms exhibit similar PRD trends reflecting that loss (PRD error) is introduced by each compression approach in a similar fashion. JPEG2000 employs an implicit thresholding step to increase the efficiency of the arithmetic encoder, while SPIHT employs a progressively decreasing threshold which governs the transmission of coefficients. Figure 5 indicates that clinically relevant information is preserved in UWB signals, allowing for classification accuracy above 80% for PRDs of up to 15%. This PRD range relates to an application where fine details in the UWB signal contain information on a tumour's shape and size.

The SPIHT algorithm encodes wavelet coefficients in order of their magnitude so that larger coefficients are prioritised over small coefficients. Smaller coefficients are therefore only transmitted if the target transmission bit-rate allows. Similarly, JPEG2000 performs compression by setting coefficients whose magnitudes are below a threshold to zero, thereby increasing the efficiency of the arithmetic encoder (by reducing the number of discrete symbols that must be encoded). With UWB, like many other real world signals, most of the signal's energy is contained in the low frequency part of the spectrum. Consequently the majority of large wavelet coefficients represent the low-frequency portion of the signal. Since JPEG2000 and SPIHT prioritise the transmission of large coefficients, the net effect of compression is that smaller high-frequency signal components are suppressed. By varying the compression ratios at which JPEG2000 and SPIHT are applied, it is possible to identify the compression algorithms' tolerance for removing smaller, mainly high-frequency, coefficients.

Future work will investigate the application of compression to applications which are not so sensitive to the shape but rather the energy of the signal.

ACKNOWLEDGMENT

REFERENCES

1. Lazaro, A., D. Girbau, and R. Villarino, "Simulated and experimental investigation of microwave imaging using UWB," *Progress In Electromagnetics Research*, Vol. 94, 263–280, 2009.

2. O'Halloran, M., E. Jones, and M. Glavin, "Channel-ranked beamformer for the early detection of breast cancer," *Progress In Electromagnetics Research*, Vol. 103, 153–168, 2010.

3. Maskooki, A., E. Gunawan, C. B. Soh, and K. S. Low, "Frequency domain skin artifact removal method for ultra-wideband breast cancer detection," *Progress In Electromagnetics Research*, Vol. 98, 299–314, 2009.

4. AlShehri, S. A. and S. Khatun, "UWB imaging for breast cancer detection using neural network," *Progress In Electromagnetics Research C*, Vol. 7, 79–93, 2009.

5. Zainud-Deen, S. H., W. M. Hassen, E. El Deen Ali, and K. H. Awadalla, "Breast cancer detection using a hybrid finite difference frequency domain and particle swarm optimization techniques," *Progress In Electromagnetics Research B*, Vol. 3, 35–46, 2008.

6. Zhou, H., T. Takenaka, J. Johnson, and T. Tanaka, "A breast imaging model using microwaves and a time domain three dimensional reconstruction method," *Progress In Electromagnetics Research*, Vol. 93, 57–70, 2009.

7. Fear, E., J. Sill, and M. Stuchly, "Microwave system for breast tumor detection: experimental concept evaluation," *IEEE AP-S International Symposium and USNC/URSI Radio Science Meeting*, Vol. 1, 819–822, San Antonio, Texas, June 2002.

8. Khalaj Amineh, R., A. Trehan, and N. K. Nikolova, "TEM horn antenna for ultra-wide band microwave breast imaging," *Progress In Electromagnetics Research B*, Vol. 13, 59–74, 2009.

9. Li, X. and S. C. Hagness, "A confocal microwave imaging algorithm for breast cancer detection," *IEEE Microwave and Wireless Components Letters*, Vol. 11, No. 3, 130–132, 2001.

10. Li, X., E. J. Bond, B. D. V. Veen, and S. C. Hagness, "An overview of ultra-wideband microwave imaging via space-time beamforming for early-stage breast-cancer detection," *IEEE Antennas and Propagation Magazine*, Vol. 47, No. 1, 19–34, February 2005.

11. O'Halloran, M., E. Jones, and M. Glavin, "Effects of fibroglandular distribution on data-independent beamformering algorithms," *Progress In Electromagnetics Research*, Vol. 97, 141–158, 2009.

12. O'Halloran, M., M. Glavin, and E. Jones, "Quasi-multistatic MIST beamforming for the early detection of breast cancer," *IEEE Trans. Biomed. Eng.*, Vol. 57, No. 4, 830–840, 2009.

13. Zhang, H., S. Tan, and H. Tan, "A novel method for microwave breast cancer detection," *Progress In Electromagnetics Research*, Vol. 83, 413–434, 2008.

14. Bindu, G., S. J. Abraham, A. Lonappan, V. Thomas,

C. K. Aanandan, and K. T. Mathew, "Active microwave imaging for breast cancer detection," *Progress In Electromagnetics Research*, Vol. 58, 149–169, 2006.

15. Conceicao, R. C., M. O'Halloran, M. Glavin, and E. Jones, "Support vector machines for the classification of early-stage breast cancer based on radar target signatures," *Progress In Electromagnetics Research B*, Vol. 23, 311–327, 2010.

16. McGinley, B., M. O'Halloran, R. C. Conceicao, F. Morgan, M. Glavin, and E. Jones, "Spiking neural networks for breast cancer classification using radar target signatures," *Progress In Electromagnetics Research C*, Vol. 17, 79–94, 2010.

17. O'Halloran, M., B. McGinley, R. C. Conceicao, F. Morgan, E. Jones, and M. Glavin, "Spiking neural networks for breast cancer classification in a dielectrically heterogeneous breast," *Progress In Electromagnetics Research*, Vol. 113, 413–428, 2011.

18. Ziganshin, E., M. Numerov, and S. Vygolov, "UWB baby monitor," *2010 5th International Conference on Ultrawideband and Ultrashort Impulse Signals (UWBUSIS)*, 159–161, 2010.

19. Staderini, E., "UWB radars in medicine," *IEEE Aerospace and Electronic Systems Magazine*, Vol. 17, No. 1, 13–18, January 2002.

20. Chia, M., S. Leong, C. Sim, and K. Chan, "Through-wall UWB radar operating within fcc's mask for sensing heart beat and breathing rate," *European Radar Conference, 2005 (EURAD 2005)*, 267–270, 2005.

21. Zito, D., D. Pepe, B. Neri, and D. De Rossi, "Feasibility study of a low-cost system-on-a-chip UWB pulse radar on silicon for the heart monitoring," *2007 International Waveform Diversity and Design Conference*, 32–36, 2007.

22. Otto, C., A. Milenkovic, C. Sanders, and E. Jovanov, "System architecture of a wireless body area sensor network for ubiquitous health monitoring," *Journal of Mobile Multimedia*, Vol. 1, No. 4, 307–326, 2006.

23. Adams, M. "The JPEG-2000 still image compression standard," *ISO/IEC JTC 1/SC 29/WG 1 N 2412.*, Citeseer, 2001.

24. Said, A. and W. Pearlman, "A new, fast, and efficient image codec based on set partitioning in hierarchical trees," *IEEE Transactions on Circuits and Systems for Video Technology*, Vol. 6, No. 3, 243–250, 2002.

25. Unser, M. and A. Aldroubi, "A review of wavelets in biomedical applications," *Proceedings of the IEEE*, Vol. 84, No. 4, 626–638, 2002.

26. Mallat, S., *A Wavelet Tour of Signal Processing*, Academic Press, 1999.

27. Daubechies, I., "Orthonormal bases of compactly supported wavelets," *Communications on Pure and Applied Mathematics*, Vol. 41, No. 7, 909–996, 1988.

28. Graps, A., "An introduction to wavelets," *IEEE Computational Science & Engineering*, Vol. 2, No. 2, 50–61, 1995.

29. ISO/IEC 15444-1:2000, ISO — International Organization for Standardization Std., 2000.

30. Higgins, G., S. Faul, R. McEvoy, B. McGinley, M. Glavin, W. Marnane, and E. Jones, "EEG compression using JPEG2000: How much loss is too much?" *2010 Annual International Conference of the IEEE Engineering in Medicine and Biology Society (EMBC)*, 614–617, 2010.

31. Nguyen, M. and R. Rangayyan, "Shape analysis of breast masses in mammograms via the fractial dimension," *Engineering in Medicine and Biology 27th Annual Conference.*, 3210–3213, 2005.

32. Muinonen, K., "Introducing the gaussian shape hypothesis for asteroids and comets," *Astronomy and Astrophysics*, Vol. 332, 1087–1098, 1998.

33. Muinonen, K., *Light Scattering by Stochastically Shaped Particles.*, Chapter 11, Academic Press, 2000.

34. Davis, S. K., B. D. V. Veen, S. C. Hagness, and F. Kelcz, "Breast tumor characterization based on ultrawideband backscatter," *IEEE Trans. Biomed. Eng.*, Vol. 55, No. 1, 237–246, 2008.

35. Taflove, A. and S. C. Hagness, *Computational Electrodynamics: The Finite-difference Time-domain Method*, Artech House Publishers, June 2005.

36. Cohen, A., I. Daubechies, and J. Feauveau, "Biorthogonal bases of compactly supported wavelets," *Communications on Pure and Applied Mathematics*, Vol. 45, No. 5, 485–560, 1992.

37. Lu, Z., D. Kim, and W. Pearlman, "Wavelet compression of ECG signals by the set partitioning in hierarchical trees algorithm," *IEEE Transactions on Biomedical Engineering*, Vol. 47, No. 7, 849–856, 2002.

38. Hilton, M., "Wavelet and wavelet packet compression of electrocardiograms," *IEEE Transactions on Biomedical Engineering*, Vol. 44, No. 5, 394–402, 2002.